Time-Resolved High-Energy X-Ray Spectra of Laser-Irradiated Targets

Peter Hoong-Yee Lee and Mordecai David Rosen
Lawrence Livermore Laboratory, University of California, Livermore, California 94550
(Received 29 August 1978)

Temporally resolved x-ray spectra in the range of 1–20 keV have been obtained from laser-irradiated high-Z disk targets. We obtain the first time-resolved direct observation of the suprathermal x-ray tail resulting from hot-electron generation due to collective processes. The measurements indicated that the suprathermal temperature θ_H has a temporal behavior which essentially follows the laser pulse of intensity I, implying a relation $\theta_H \sim I^n$, $n \gtrsim 1$, an unexpected result.

In laser-produced plasmas, most of the electromagnetic radiation that the plasma emits is in the soft-x-ray regime. The x rays generated from bremsstrahlung and recombination radiation yield direct information on the electron temperature. On the other hand, suprathermal or "hot" electrons are generated by the resonance-absorption mechanism[1-3] as well as other collective phenomena such as parametric decay and oscillating two-stream instabilities.[4-7] Time-integrated "hot" x-ray emissions arising from the nonthermal high-energy tail on the electron energy distribution have been observed in laser-plasma interaction experiments,[8,9] and time-integrated "temperatures" have been inferred from the slope of that tail. For ablatively driven laser-fusion targets, calculations show that suprathermal electrons generated by plasma instabilities tend to preheat the fuel and thus have a detrimental effect on target performance.[10] It is, therefore, important to study the temporal behavior of x-ray emission spectra of laser-produced plasmas. In this Letter we present the first temporally resolved x-ray emission spectra from laser-irradiated high-Z targets, which show the time evolution of both thermal and hot x-ray temperatures. The results imply a much stronger dependence of the hot temperature on the laser intensity than has previously been seen in time-integrated observations.

The experiments were performed at 1.06-μm wavelength with one beam of the Argus laser facility,[11] operating in this case with 250–350-J, 200–400-ps full width at half maximum (FWHM) pulses, the typical intensity on target being in the $1-3\times10^{15}$-W/cm^2 range. The targets consisted of gold disks, 300 μm in diameter and thicknesses in the range 10–50 μm. The instrument used for time-resolved x-ray measurements is the Livermore 15-ps x-ray streak camera, which is described elsewhere.[12] For the present purpose, an eleven-channel, K-edge filter pack was used. The foil materials of this filter pack consisted of two channel thicknesses of polyvinylchloride (chlorine, K edge at 2.8 keV), two of titanium (5 keV), two of cobalt (7.7 keV), one of zinc (9.7 keV), one of yttrium (17 keV), two of molybdenum (20 keV), and one of silver (25.5 keV). Appropriate foil thicknesses of the respective channels were chosen to provide optimum channel responses and double channels of varying thicknesses were used to accomodate the large dynamic range in emission intensities and to provide for error bar estimates in given spectral regions. The instrument response of the x-ray streak camera was calibrated at a multirange monoenergetic x-ray source from 4.5 to 98 keV, the instrument streak speed and dynamic range were calibrated on a small 1-J laser facility. From the streak records, one obtains the time-resolved x-ray emissions for each channel by using the measured instrument streak speed. By using the measured instrument response, the x-ray intensities of the different channels can be related to one another in relative intensity and provide an unfold of the x-ray emission spectra at any given time during the laser interaction with the target.[13] A typical streak record from a

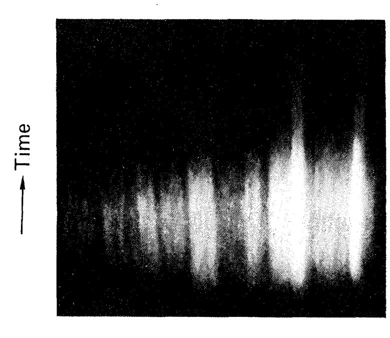

FIG. 1. A typical streak record from a target shot obtained with the x-ray streak camera by using an eleven-channel, K-edge filter pack. Channels 1 to 11 are from right to left. K-edge energies are ~3–25 keV.

target shot obtained with the eleven-channel filter pack is shown in Fig. 1.

We note that the peak emission of all eleven channels occur at the same time. The duration and temporal shape of the x-ray emission pulses, however, are different. The hot x rays, i.e., emissions at energy channels higher than ~ 10 keV, have a temporal behavior which essentially follows the laser pulse. Since the energy-loss time for a hot electron at ~ 10 keV is, classically, only a few picoseconds, the hot x-ray behavior should follow the laser pulse. This is the first time-resolved direct observation of the suprathermal x-ray behavior due to hot electrons produced by collective processes.

A sample set of time-resolved high-energy x-ray spectra is shown in Fig. 2. The target was irradiated by 330-J, 400-ps (FWHM) pulse. The peak intensity for this experiment was 1.7×10^{15} W/cm^2 and the measured absorption was 20%. The time scale is chosen such that zero time refers to the time when all eleven channels have peak emmission. It is logical to presume that this peak emission time also corresponds to the peak of the laser pulse. Code simulations (discussed below) also show that peak x-ray emissions coincide with the laser peak. From Fig. 2, one can clearly see the evolution of the slope of the high-energy tail in time. The suprathermal or hot x-ray temperature, θ_H, is defined by the slope of the spectrum in the energy range above ~ 8 keV. The high-energy tail is detected at about 180 ps before peak x-ray emission, gradually increasing to a maximum θ_H value of 9 keV at the peak, and then decreasing with diminishing laser power. It is also apparent from the spectra that the thermal x-ray temperature, θ_c, defined by the slope of the spectrum in the energy range below ~ 8 keV, is decoupled from the hot x-ray temperature throughout the laser pulse, having a fairly constant value of about 0.7 keV. It should be noted that the presence of prominent gold spectral lines at around 2.5 keV makes the determination of θ_c somewhat less accurate.

A comparison of the experimental results with LASNEX[14] code predictions is shown in Figs. 3 and 4 for both the hot and thermal x-ray temperatures, respectively. The LASNEX computation is made under the assumption that inverse bremsstrahlung is the prinicpal absorption mechanism and about 20% of the remaining light that reaches the critical surface is reasonantly absorbed, creating an electron distribution, characterized by a T_H given by

$$T_H = T_B + 49.4(I\lambda^2)^{0.425}T_B^{\,0.04} \times (1 + 3T_i/ZT_B)^{0.25}, \qquad (1)$$

where T_B is the average electron temperature in keV, T_i is the ion temperature, I is the laser intensity in units of 10^{17} W/cm^2, λ is the incident

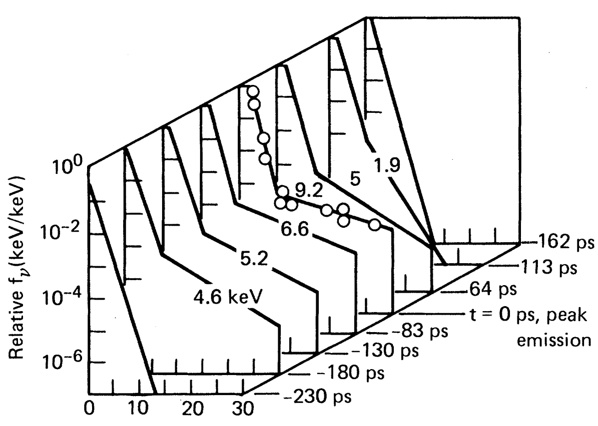

FIG. 2. Time-resolved x-ray spectra of 1.06-μm laser-irradiated Au-disk (330 J, 400 ps, 1.7×10^{15} W/cm^2). The absorption for this shot was 20%. Zero time refers to peak emission. Note the evolution of the high-energy "tail" in time.

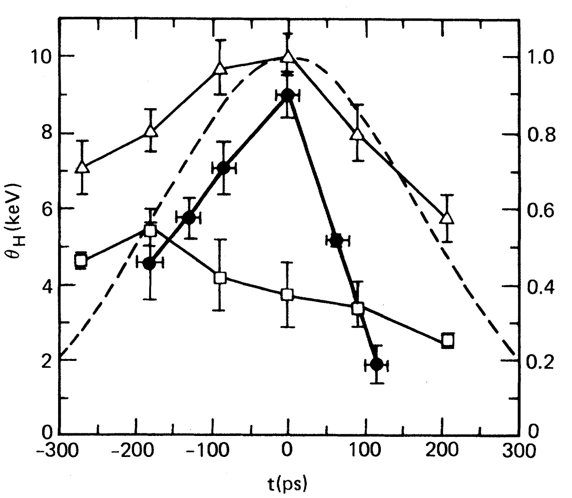

FIG. 3. Hot x-ray temperature as a function of time —a comparison of measured values and LASNEX code results. I/I_0 is the 400-ps FWHM laser-pulse intensity normalized by its peak value. No fiducial was used, but the laser pulse is chosen to have its peak matched with the peak of the x-ray emission pulse. Zero time refers to the peak. Dashed line, laser pulse; filled circle, experimental data; triangle, LASNEX, inhibited transport; square LASNEX, noninhibited transport.

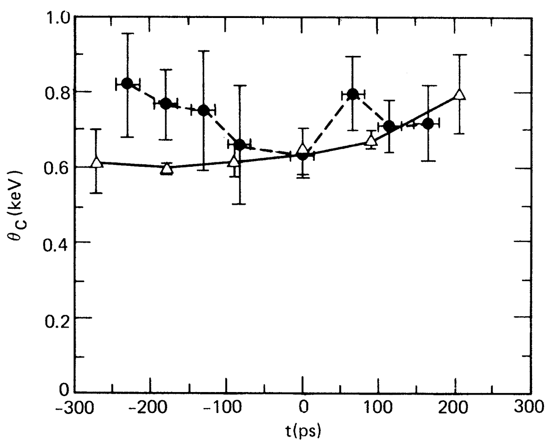

FIG. 4. Comparison of measured and LASNEX-code calculated thermal x-ray temperatures as a function of time. Note that θ_c is fairly constant throughout the laser pulse, and θ_c is decoupled from θ_H. Filled circle, experimental data; triangle, LASNEX, inhibited transport.

laser wavelength in microns, Z is the charge state of the target material at critical density, and T_H is the hot-electron temperature. Note that T_H is not the same as θ_H; θ_H is defined operationally by the slope of the code-produced x-ray spectra generated by the electrons. Equation (1) is based on particle simulations and is consistent with well-established time-integrated θ_H vs $I\lambda^2$ data.[3,15] In high-Z plasmas,[16] it is quite plausible that heat flux is inhibited by ion-acoustic turbulence, since the condition for minimal ion Landau damping $c_s \gg v_i$ is $ZT_e \gg T_i$, where c_s and v_i are the ion thermal speeds, respectively. Thus turbulence is allowed to grow and presummably saturate at $v_{\mathrm{drift}} \approx c_s$, leading to an effective inhibition of $c_s/v_e \approx 0.02$, where v_e is the electron thermal speed. When this inhibition is modeled in the code, there is qualitative agreement between code predictions and experiment (see Fig. 3, inhibitied-transport curve). The code predicts higher values before and after the peak of the pulse; however, the value of θ_H at peak emission is predicted accurately to within 10% of the measurement. On the other hand, if the heat flux is not inhibited, the plasma corona is cooled, thereby increasing the inverse bremsstrahlung, and only 10% of the incident laser light ends up as being resonantly absorbed. The noninhibited transport curve in Fig. 3 clearly shows that such a mix of absorptions does not match the observed data. [From Eq. (1), $T_H = T_B + \cdots$; T_B is much cooler in this case leading to lower T_H]. Also plotted in Fig. 3 is the laser pulse normalized by its peak value. We have chosen to match the peak of the laser pulse with the peak of the x-ray emission pulse, and we note that at this time θ_H is highest. This seems reasonable in terms of the resonance-absorption theory[1-3]; since θ_c is roughly constant, the ratio of the electron quiver velocity to the thermal velocity is maximum at the peak of the laser pulse (for $\theta_c = 0.7$ keV and $I = 1.7 \times 10^{15}$ W/cm^2, $v_{\mathrm{osc}}/v_{\mathrm{th}} \sim 1$). Consequently, the highest-energy electrons are generated at that time and therefore, the x rays should be the hottest. We note that if θ_H scales like I^n, then the measured data indicate that $n \simeq 1$ before the peak and $n \gtrsim 1$ after the peak, whereas the code using the inhibited-transport model suggests that $n < 1$ before the peak and $n \lesssim 1$ after the peak. [Of course, the code is constrained to follow the $T_H \sim I^{0.4}$ scaling prescribed by Eq. (1).] A likely explanation for n being different before and after the peak is that the plasma density profile and corona evolve in time and thus are asymmetric with respect to the peak of the laser pulse. For example, with a hotter corona the classical absorption might drop and/or Brillouin scattering can build up.[17] This enhanced scattering leads to decreased laser intensity on the critical surface, and may account for the rapid drop in θ_H. Earlier experimental and theoretical analyses[2,3] of θ_H, which suggested $n \approx \frac{1}{3}$, were based on time-integrated data, and thus reflect θ_H vs I (peak value) behavior only. Our own measurement of the *peak* time-resolved θ_H indeed matches those earlier predictions, but *throughout* the pulse, n is clearly much greater than $\frac{1}{3}$. Since most of the preheating electrons are created near the peak of the pulse, it is there that a predictive capability is most essential, and thus the earlier analyses are still quite relevant. From a basic physics point of view, however, this difference in n requires further study and understanding.

The code predictions for the thermal x-ray temperature are slightly lower than the measured values (see Fig. 4), but are in good agreement with the experiment in that θ_c is fairly constant throughout the laser pulse, while θ_H is not. This fact suggests that the behavior of the thermal electrons is governed by hydrodynamics and thermal conduction, while the suprathermal electrons follow the laser-pulse time scale when collective processes are effective.

Independent measurements on this particular experiment with a different diagnostic yield time-integrated data[18] of $\theta_c = 0.7 \pm 0.15$ keV which is in agreement with the x-ray streak-camera data as well as the code predictions here. However, the time-integrated θ_H is 14.1 ± 3 keV, which is somewhat high. There are numerous other shots where the correspondence between the time-integrated and the time-resolved data of θ_H are much better, with differences between 5–30%.

In conclusion, we have succeeded in obtaining time-resolved high-energy x-ray spectra by using an x-ray spectra by using an x-ray streak camera with multichannel filter packs. We have observed both the thermal and suprathermal x-ray temperature evolve in time. We have observed that θ_H follows the laser pulse on grounds explainable by collective plasma processes but θ_c remains fairly constant and decoupled from θ_H. We also note that the θ_H dependence on laser intensity is much stronger than has been previously assumed. We speculate that this may be due to enhanced Brillouin scattering since it can cause the laser intensity *at critical* to drop off more sharply in time than the temporal Gaussian of the incident pulse.

We are expecially indebted to D. T. Attwood for many helpful and stimulating discussions. The authors acknowledge the material support and encouragement of their many colleagues in the Livermore Laser Fusion Program, in particular, K. G. Estabrook, H. N. Kornblum, E. L. Pierce, M. J. Boyle, E. M. Campbell, H. G. Ahlstrom, and E. K. Storm. This work was performed under the auspices of the U. S. Department of Energy under Contract No. W-7405-Eng-48.

[1]K. G. Estabrook E. J. Valeo, and W. L. Kruer, Phys. Fluids 18, 1151 (1975).
[2]D. W. Forslund, J. M. Kindel, and K. Lee, Phys. Rev. Lett. 39, 284 (1977).
[3]K. Estabrook and W. L. Kruer, Phys. Rev. Lett. 40, 42 (1978).
[4]K. Mizuno and J. S. DeGroot, Phys. Rev. Lett. 35, 219 (1975).
[5]J. Denavit, Phys. Fluids 19, 972 (1976).
[6]W. L. Kruer and J. M. Dawson, Phys. Fluids 15, 446 (1972).
[7]J. I. Katz *et al.*, Phys. Fluids 16, 1519 (1973).
[8]R. A. Haas *et al.*, Phys. Fluids 20, 322 (1977).
[9]E. K. Storm *et al.*, Phys. Rev. Lett. 40, 1570 (1978).
[10]J. Nuckolls *et al.*, Nature (London) 239, 139 (1972).
[11]W. W. Simmons *et al.*, Appl. Opt. 17, 999 (1978).
[12]D. T. Attwood *et al.*, Phys. Rev. Lett. 37, 499 (1976).
[13]P. H. Y. Lee *et al.*, Bull. Am. Phys. Soc. 22, 1113 (1977).
[14]G. B. Zimmerman, Lawrence Livermore Laboratory Report No. UCRL-76927, 1975 (unpublished).
[15]K. G. Estabrook, private communications.
[16]M. D. Rosen *et al.*, Lawrence Livermore Laboratory Laser Program Annual Report, 1977 (to be published).
[17]D. W. Phillion, W. L. Kruer, and V. C. Rupert, Phys. Rev. Lett. 39, 1529 (1977).
[18]H. N. Kornblum, private communications.

Double-Diffusion Hot-Electron Transport in Self-Consistent E and B Fields

R. J. Mason
Laser Division, Los Alamos Scientific Laboratory, Los Alamos, New Mexico 87545
(Received 5 July 1978)

A two-component, flux-limited diffusion model is introduced for the self-consistent transport of hot electrons in laser-produced plasmas. Megagauss fields from the $\nabla n_h \times \nabla n_c$ source are predicted for $I\lambda^2 \gtrsim 3\times 10^{16}$ W μm^2/cm^2. For low-Z target materials a prompt back-side B field is a signature for hot electrons reaching the back of thin foils.

Recent experiments reconfirm the existence of megagauss magnetic fields[1] in laser-produced plasmas. X-ray data imply[2] that the hot-electron density exceeds 50% of critical for $I\lambda^2 \gtrsim 7\times 10^{15}$ W μm^2/cm^2. Generally, B-field treatments have involved the transport of a single thermal-electron component.[3,4] Novel suprathermal treatments have recently appeared,[5,6] but these are confined to one-dimensional applications. Zimmerman[7] does multigroup suprathermal transport in the code LASNEX, but only selected magnetic effects are included,[8] e.g., there is no $\nabla n_h \times \nabla n_c$ hot-electron B-field source. Colombant and Tidman[9] have discussed the field from such a source, but they neglect $\omega\tau$ effects and avoid a transport analysis. The present Letter gives the first results for the self-consistent transport of hot and cold electrons with E and B fields.

Model equations.—A simulation code has been constructed in which the hot and cold electrons

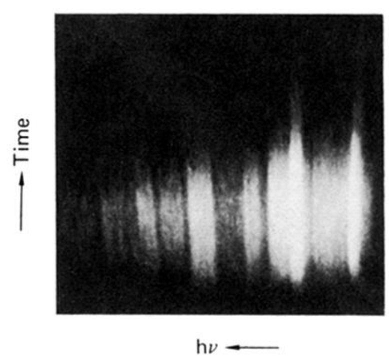

FIG. 1. A typical streak record from a target shot obtained with the x-ray streak camera by using an eleven-channel, K-edge filter pack. Channels 1 to 11 are from right to left. K-edge energies are ~3–25 keV.